EVALUATION OF NPL CSF1 FREQUENCY STANDARD

K. Szymaniec, W. Chalupczak, D. Henderson

National Physical Laboratory,
Queens Road, Teddington, TW11 0LW, UK

Keywords: atomic frequency standard, laser cooling, caesium fountain.

Abstract

In this contribution a new caesium fountain frequency standard at the National Physical laboratory (NPL-CsF1) is described. Procedures for evaluation of the systematic frequency shifts are presented. The NPL-CsF1 has a short-term stability of $1.4\times10^{-13}\ \tau^{-½}$, predominantly due to the local oscillator phase noise. The accuracy, of 1 part in 10^{15} is limited by the uncertainty of the frequency shift due to collisions between cold atoms.

1 Introduction

A new generation of primary frequency standards (PFS), based on atomic fountains, has become operational, following the development of techniques in laser cooling and manipulation of atoms [1-4]. In atomic fountains, laser cooled atoms are launched upward, rising about a metre, resulting in an increased interaction time, on the order of a second. Consequently, the line Q-factor of 10^{10}, higher than in conventional beam clocks, has led to substantial improvements in the performance of PFSs. A short-term stability of $10^{-13}\ \tau^{-½}$ and an accuracy of 1 in 10^{15} are typical for these devices, with scope for improvement of another order of magnitude. To date, four National Measurement Institutes have been contributing to the evaluations of the TAI time interval using a fountain PFS. The contribution of these fountain PFSs is leading to the international time scale, TAI being a more accurate representation of Terrestrial Time (whose step interval is the SI second). In addition, several further NMIs have been developing atomic fountains.

At the National Physical Laboratory, a new caesium fountain standard (NPL-CsF1) is now operational [5]. In the last year an evaluation of the stability and the systematic frequency shifts has been conducted on NPL-CsF1. At the same time, NPL-CsF1 has been linked to the NPL time scale (UTC(NPL)) and has been used for direct measurements of optical frequency standards that are under development.

NPL-CsF1 is described in Section 2, including an analysis of the detection noise and the short-term stability. The identified systematic effects are listed in Section 3, together with estimates of their uncertainties. Results of frequency measurements and comparisons are presented in Section 4, followed by conclusions in Section 5.

2 Description of the apparatus

In NPL-CsF1, atoms are collected and cooled in a magneto-optical trap (MOT). They are launched and cooled further as a moving molasses. During their ballistic flight the atoms twice pass through a microwave cavity (Ramsey cavity). The two microwave interactions, together with the intervening period (Ramsey time) constitute a Ramsey interaction. The atomic state after the Ramsey interaction is detected by means of laser induced fluorescence. The detection of the distribution of the atom population between the hyperfine components of the ground state is highly efficient, as each atom scatters 10^4 photons during the process.

The NPL-CsF1 apparatus can be divided into the following parts: the vacuum vessel with magnetically shielded flight tube, the laser system, the source of the interrogating microwave field and the electronics for data acquisition and control of the experiment.

2.1 Vacuum vessel

There are three functional sections of the vacuum system (see Fig.1): the trapping and cooling region in the centre; the flight tube above, containing the Ramsey cavity; and the detection chamber below.

The cooling chamber is constructed from an A316 stainless-steel 6-way DN63 cross, modified with an additional 4 arms in the horizontal plane, fitted with DN40 flanges. A total of 8 view-ports are mounted on the horizontal arms, providing access for cooling lasers, for MOT diagnostics and for the microwaves used for the selection of the m_F=0 population. Two additional view-ports provide access along the vertical direction. The (0,0,1) cooling geometry is used, with two horizontal pairs of counter-propagating beams and one vertical pair. The central cross is connected to a reservoir containing a 5g ampoule of caesium. A Cs vapour at a pressure of 10^{-6} Pa is maintained in the trapping and cooling region. The transition pieces connecting the flight tube and the detection chamber are lined with graphite tubes serving as getter pumps to minimize the Cs pressure outside the cooling chamber. A set of anti-Helmholtz coils is mounted between the vertical flanges of the 10-way cross, to produce a field gradient of 1.0 mT/cm for the MOT. An additional three pairs

of coils are used to reduce the effect of the Earth's magnetic field to less than 0.2 μT.

The flight tube, above the cooling region, is made from aluminium and has a diameter of 20 cm. A doubly wound, 72 cm long solenoid is placed immediately outside the flight tube to produce a highly uniform magnetic field (C-field), required to define the quantisation axis and to separate the magnetic components of the Cs ground state hyperfine transition. A microwave cavity, made of OFHC copper, is mounted 18 cm above the lower end of the flight tube. In order to isolate it thermally from the vacuum vessel, the cavity is held on a ceramic plate, which is supported by four aluminium rods. The flight tube is screened from undesired magnetic fields; three layers of magnetic shielding surround the flight tube, each a mu-metal cylinder with 2 mm thick walls.

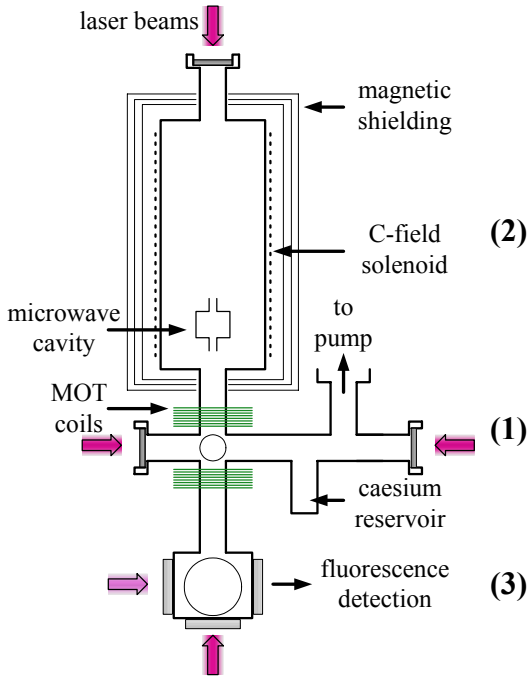

Fig 1: Schematic layout of the Cs-F1 vacuum vessel.

The detection chamber is a DN63 cube with five view-ports, providing access for detection laser beams and for fluorescence collection optics.

The vacuum vessel is pumped by two 50 l/s ion pumps maintaining the background pressure (outside the MOT region) below 10^{-7} Pa.

2.2 Lasers and optical system

Lasers operating at 852 nm (Cs D2 line) are used to capture, cool, manipulate and detect the caesium atoms. One extended cavity diode laser (ECDL) is frequency stabilised to the F=4→F'=5 transition using a saturated absorption signal from a room temperature Cs cell and the FM locking technique. A small part of its output is amplified in four slave diodes by injection locking, to provide cooling beams, while the remainder is used for detection. A second ECDL is stabilised, in the same way as the first, to the F=3→F'=4 transition. This laser provides repumping light for both cooling and detection. The detuning and intensity of the cooling light is controlled by acousto-optic modulators in a double pass configuration. In addition, mechanical shutters are used to eliminate residual scattering of resonant light during the Ramsey time. Polarisation-maintaining optical fibres transfer the cooling and repumping light to the fountain from a separate optical table. At the output of the fibres the cooling beams are collimated to an $e^{-1/2}$ diameter of 1.5 cm with a peak intensity of 5 mW/cm^2. One of the vertical beams is truncated to 1 cm diameter by the aperture in the Ramsey cavity.

Detection is carried out by collecting fluorescence from the cycling transition, F=4→F'=5. A polarising fibre transmits the detection beam directly from the ECDL laser to the detection chamber. There, it is collimated and split into two beams, each shaped into a rectangular cross-section of 0.8×2.0 cm. The beams are circularly polarised and retro-reflected. The lower part (approximately 1/3) of the upper beam is blocked at the retro-mirror so that the resulting travelling wave removes, by radiation pressure, the F=4 atoms fluorescing in the upper beam. The repumper light is combined with the lower detection beam; the F=3 atoms are pumped to the F=4 state and scatter photons on the cycling transition F=4→F'=5. Approximately 3% of the light scattered in the two detection zones is imaged onto two photodiodes, one dedicated to each detection channel.

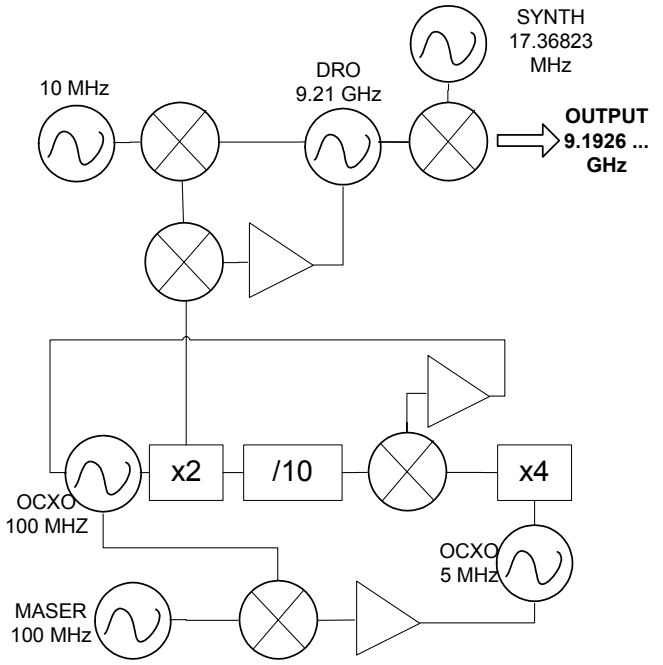

Fig. 2: Diagram of the 9.2 GHz synthesis.

2.3 Microwave interrogation

Figure 2 illustrates the local oscillator (LO) synthesis for Ramsey interaction. The microwave output is produced by

mixing a dielectric resonant oscillator (DRO) with an HP3325B synthesizer. The DRO is phase-locked to a hydrogen maser. There are two intermediate oscillators, each phase-locked with individual time constants chosen to optimise the phase noise at all offsets from the 9.192 GHz carrier. The frequency of the maser is continuously measured against UTC(NPL).

A sampling-downconverter is used to phase-lock the DRO to the doubled output of a 100 MHz oven-controlled crystal (OCXO), in an offset loop, using a second HP3325B synthesizer. The 100 MHz OCXO is locked to the 5 MHz OCXO, using a digital divider. The 5 MHz OCXO is locked to the hydrogen maser by a phase measurement of the (locked) 100 MHz OCXO. Both HP3325B synthesizers were phase locked to the hydrogen maser via the 5 MHz OCXO.

By replacing the 10 MHz synthesizer with 7.368 MHz, and omitting the final mixer, the synthesis scheme is easily adapted to produce an offset lock where the DRO runs directly on the caesium resonance. This arrangement provides higher power and was used to explore the susceptibility of the fountain to stray "leakage" fields at the caesium resonance frequency.

2.4 Fountain operation and data acquisition

The NPL-CsF1 operates in a sequence, with the following steps: collection of atoms in the MOT; launching and cooling in optical molasses; state selection; Ramsey interaction; and detection. A typical cycle lasts 1.5 s.

Around 10^8 atoms is loaded into the MOT in 550 ms. Then, before launching, a 50 ms delay allows the eddy currents induced in the magnetic shields to decay. During the first 10 ms of the delay, the cooling lasers are off, to avoid any displacement of the atomic cloud by uncontrolled magneto-optical forces. As the atoms are still relatively hot (40 μK) the cloud expands, in the dark, to approximately 1 cm diameter. The reduction of the atomic number density improves the efficiency of the cooling in the molasses phase and lowers the collisional frequency shift during the Ramsey time. To launch the atoms, the descending and ascending vertical beams are detuned by –4.8 MHz and +4.8 MHz respectively. To optimise the launch efficiency, the horizontal beams are turned off for 0.3 ms. Once the horizontal beams are restored, the intensities of all the cooling beams are slowly reduced and their detuning increased from 2 Γ to 8 Γ . Within 1.4 ms a temperature of 2 μK is reached and then all the cooling light is extinguished.

At this stage the atomic population is approximately evenly distributed among all the magnetic sublevels of the F=4 state, with about 12% of the population in the m_F=0 state. These atoms are transferred, with 95% efficiency, to the (F=3, m_F=0) state by a 5 ms pulse of a travelling microwave. Atoms remaining in the F=4 are pushed by the radiation pressure from a 0.5 ms pulse of a vertical beam, tuned to the resonance. The selected (F=3, m_F=0) atoms continue their flight into the magnetically shielded flight tube. To avoid mixing of the magnetic sublevels near the shields' end-caps, where the magnetic field is highly inhomogeneous, additional loops of current are employed. The apogee of the ballistic flight is 31 cm above the Ramsey cavity centre, giving more than 0.5 s between interactions with the microwave field and hence Ramsey fringes narrower than 1 Hz.

After completion of the Ramsey interaction some 10^6 atoms reach the detection region. As described earlier, atomic populations of the F=4 and F=3 states are detected by the upper and lower detection beams, respectively. The normalised fraction of the F=4 atoms, $N_4/(N_4+N_3)$, is used as the measure of the probability of transition, F=3→F=4, during the Ramsey interaction.

The central Ramsey fringe is used to lock the frequency, ν, of the LO to the Cs resonance. Every fountain cycle the LO frequency is toggled between ν+Δν/2 and ν-Δν/2 (where Δν is the full width at half maximum of the fringe). The transition probability for F=3→F=4 is measured and the difference between the LO frequency and the Cs frequency is calculated every two cycles. This frequency correction is then fed back to the LO.

The feedback is provided by digital control of the synthesiser whose nominal frequency is 17.36823 MHz. The mean difference of that synthesiser from 17.36823 MHz is used to calculate the fractional frequency difference of the maser from the SI frequency, taking account of the known offsets in the caesium resonance. The values for the synthesis offset, during a measurement session, are recorded for later analysis.

2.5 Short-term stability

The frequency measurement data are subject to noise due to the detection and the microwave generation processes. Fig. 3 shows the Allan deviation of the NPL-CsF1 frequency with a hydrogen maser (Datum MHM 2010) used as a reference. For predominantly white noise processes, the Allan deviation $\sigma_y(\tau)$ can be estimated from the measured signal-to-noise ratio (*S/N*) according to:

$$\sigma_y(\tau) = \frac{2}{\pi}\frac{1}{Q}\left(\frac{S}{N}\right)^{-1}\sqrt{\frac{T_c}{\tau}} \qquad (1)$$

where T_C is the duration of a single fountain cycle and τ is the averaging time. For the fountain operating at the top of the Ramsey fringe (where the LO noise contribution is negligible), the *S/N* exceeds 1000. The *S/N* is, however, reduced to 600 if measured on the slope of the fringe, due to the contribution from the phase noise of the LO. The resulting value of $\sigma_y(\tau) = 1.4\times10^{-13}\ \tau^{-½}$, is in very good agreement with that obtained experimentally.

The Allan deviation departs from the $\tau^{-1/2}$ dependence for averaging times longer than 10^4 seconds (fig. 3). This is due to hydrogen maser instabilities and drift. These instabilities can be a limitation for some comparative measurements of systematic effects, when long averaging times are required to

achieve sufficient statistical resolution. In such cases the fountain is operated in a different sequence, where one (and only one) parameter is alternated between two values every two cycles (alternating mode). Two separate subsets of measured frequencies are collected and one subset is compared (referenced) to the other. Figure 4 shows the Allan deviation of such a measurement, where the fountain was operating, respectively, at high and low density. The poorer value of the short-term stability is expected as, for each data subset, only half as many data points is acquired in a given time compared with the non-alternating mode.

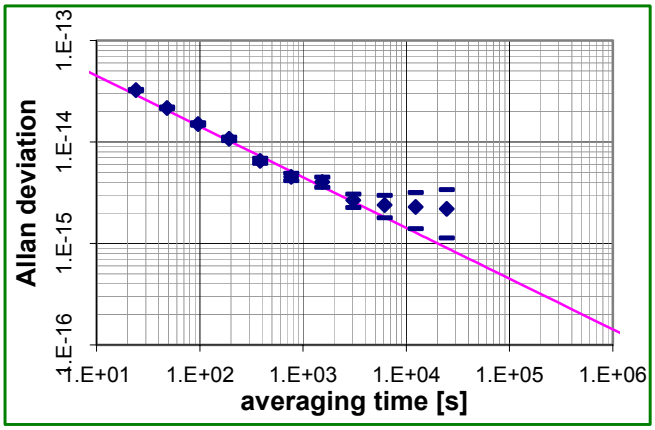

Fig. 3: Allan deviation of the frequency difference NPL-CsF1–HM3 between the fountain and maser HM3. For averaging times over 10^4 s the maser instabilities dominate.

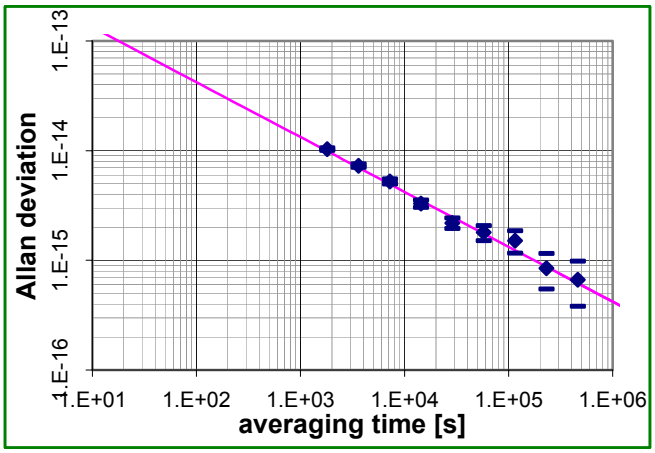

Fig. 4: Allan deviation of the frequency difference between two data subsets recorded during operation in the alternating mode. The short-term stability is poorer ($4\times10^{-13}\ \tau^{-1/2}$), but longer term stability is not limited by maser drift.

3 Systematic frequency shifts and their uncertainties

The frequency of the Cs ground state hyperfine transition is offset from that of the unperturbed transition by several systematic effects. These offsets are evaluated, together with their uncertainties. Some make a negligible contribution to the total offset; however, their uncertainty contributes to the total uncertainty. A list of systematic effects, identified for NPL-CsF1, is given below.

3.1 Second order Zeeman effect

The frequency of the "clock" transition ($F=3,m_F=0 \rightarrow F=4,m_F=0$), although free from the linear Zeeman shift, must be corrected for the quadratic shift resulting from the applied static magnetic field in the flight tube. This correction is calculated using measurements of the frequency shift of the field-sensitive transition ($F=3,m_F=1 \rightarrow F=4,m_F=1$), denoted by $f_{1-1}^{(1)}$. In general, frequencies of hyperfine transitions in the presence of an external static magnetic field are given by the Breit-Rabi formula [6]:

$$\nu_{(3,m_F\rightarrow 4,m_F)} = \nu_0\left[1+\frac{m_F}{4}x+\left(1-\left(\frac{m_F}{4}\right)^2\right)\frac{x^2}{2}+\ldots\right] \qquad (2)$$

where the parameter x is given by:

$$x=(g_j-g_i)\mu_B B/(h\nu_0) \qquad (3)$$

and B is the magnetic field induction. The relation between the linear frequency shift $f_{1-1}^{(1)}$ and the required quadratic shift of the clock transition can be derived from (2):

$$f_{0-0}^{(2)} = 8\cdot\left(f_{1-1}^{(1)}\right)^2 \qquad (4)$$

The shifts are fractional frequency shifts, relative to ν_0, and the quadratic contribution to the shift of the $(3,1\rightarrow4,1)$ transition is neglected.

Using the Ramsey interaction, a time-averaged value of the linear Zeeman shift is obtained and $\left\langle f_{1-1}^{(1)}\right\rangle^2$ is used to calculate $f_{0-0}^{(2)}$ from the formula (4). However, a bias is introduced to $f_{0-0}^{(2)}$, if the atoms experience an inhomogeneous magnetic field. A measure of the inhomogeneity is given by the variance:

$$\left\langle\left(f_{1-1}^{(1)}\right)^2\right\rangle-\left\langle f_{1-1}^{(1)}\right\rangle^2=\sigma_f^2 \qquad (5)$$

and the bias is equal to $8\times\sigma_f^2$.

It is possible to map the magnetic field by launching the atomic cloud to various heights and measuring the frequency $\left\langle f_{1-1}^{(1)}\right\rangle$ (see fig. 5). The values of $f_{1-1}^{(1)}$ for each point above the cavity can then be calculated, whereupon $\left\langle\left(f_{1-1}^{(1)}\right)^2\right\rangle$ can be calculated from the atoms' trajectory. In NPL-CsF1 the

bias introduced by inhomogeneity in the magnetic field is at the 10^{-19} level and is neglected.

For non-monokinetic atomic samples, the contrast of the Ramsey pattern is reduced; interference occurs due to groups of atoms with different velocities having different Ramsey interaction times. The interference causes the contrast to be reduced towards the tail of the Rabi envelope. For fringes measured on the (3,1→4,1) transition, this effect, together with a small variation of *B* over the ballistic trajectory, results in a displacement of the central fringe from the centre of the Rabi pedestal. Therefore, the field mapping procedure of launching the atomic cloud to various heights is used to identify the central Ramsey fringe.

The uncertainty of the frequency correction due to the second order Zeeman effect is dominated by the temporal instability of *B*. The temporal peak-to-peak variation of *B* is less than 30 pT over several weeks of fountain operation, leading to an uncertainty of less than 5×10^{-17}.

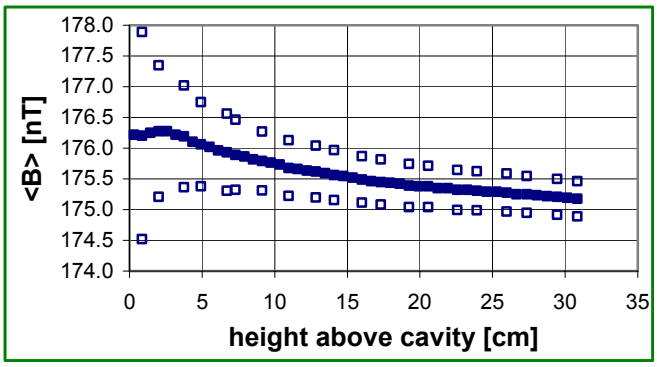

Fig. 5: The time integral of the magnetic field over the path, for atoms launched to different heights <*B*> (full squares). The magnetic field values are calculated from the positions of the central Ramsey fringe for the (3,1→4,1) transition. To avoid misinterpretation of the fringes, the values of <*B*> calculated for fringes adjacent to the central one are also shown (open squares).

3.2 Frequency shift due to collisions

Collisions between cold caesium atoms give rise to a shift of the frequency of the "clock" transition [7]. Theoretical calculations show that the shift displays a resonant dependence on the temperature of colliding atoms for samples cooled to about 100 nK [8]. In NPL-CsF1, however, where the temperature of the launched atoms is 1-2 μK, the approximation is made that the collisional frequency shift is proportional only to the atomic number density in the cloud. An extrapolation of the frequency, as directly measured, to the zero-density value is problematic, for two reasons. First, there is only a limited range over which the atomic density can be varied without a significant degradation of the *S/N*. (A density reduction by factor of 2 does not significantly change the stability, as the short-term of NPL-CsF1is dominated by the LO.) Second, the atomic density is not controlled directly; the detected fluorescence is controlled and hence the number of atoms N_{at}, reaching the detection zone (to the extent that the detection process is linear). A technique to link, unambiguously, changes in density with changes in N_{at} has recently been demonstrated [9]. In the current configuration of NPL-CsF1 it is not possible to implement that technique. However, it is possible to demonstrate the linearity between N_{at} and the frequency shift. In fig. 6 fractional frequency differences between NPL-CsF1 and one of our masers (HM3) are plotted for several values of N_{at}. The number of detected atoms was varied by changing only the power or detuning of the selecting pulse. Other parameters, such as the MOT loading time or the intensity of the cooling beams remained, unchanged. Given the statistical uncertainty of the data collected for each value of N_{at}, it is possible to calculate the uncertainty of the intercept for $N_{at}=0$. From this uncertainty it is estimated that, by applying a linear dependence between N_{at} and the collisional frequency shift, the extrapolation procedure may lead to a systematic bias not greater than 8×10^{-16}.

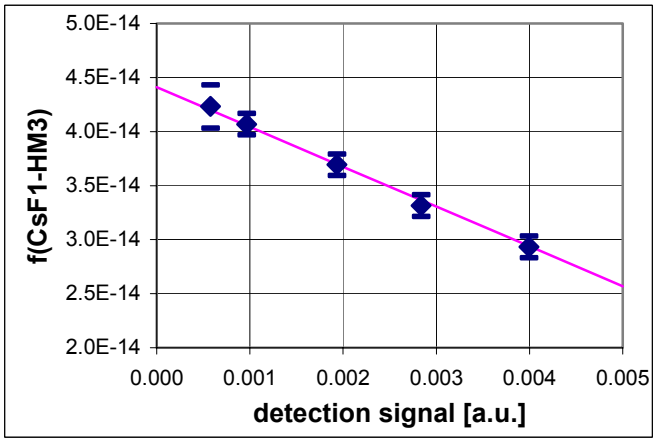

Fig. 6: The fractional frequency difference NPL-CsF1–HM3 as a function of the detected atom number N_{at}. The maser frequency drift over the measurement time was removed. The straight line is a least square fit to the experimental data.

It should be noted that no use is made of the linear fit from fig. 6 as a transfer function between the detection signal and the correction for the spin-exchange shift; the utility of the linear fit is solely to validate our extrapolation procedure. During a measurement campaign the fountain is operated continuously in the alternating mode, correcting for the collisional shift (see Section 4). The LO corrections together with N_{at} are recorded for the two sets of data corresponding to the high and low atom number densities. Typically, the fountain data is averaged in 30-minute blocks and the extrapolated frequency is calculated from the averaged ratio between signals, for the high and low density respectively (fig. 7). (The 30-minute averaging time is chosen in order that

the noise from the H-maser reference is white frequency noise, before the flicker-floor is reached, and makes a negligible contribution.) The accuracy of the measurement is not affected by the long-term stability of either the atom number or the ratio. Nevertheless, the N_{at} detection signal is stable within 10% over a 30-day measurement campaign.

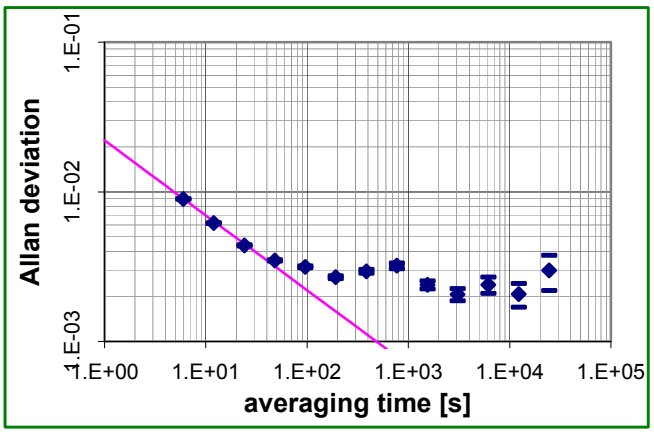

Fig. 7: The stability of the atom number ratio. For averaging times over 100 seconds it is better than 0.5%. The correction for collisional shift is calculated every 1800 seconds.

The NPL-CsF1 operates at a background pressure below 10^{-7} Pa. At this level the frequency shift caused by collisions with molecules of the background gas [10] is two orders of magnitude smaller than that due to the collisions with cold caesium atoms and being negligible, is omitted from the uncertainty budget.

3.3 Black-body radiation

Assuming that a 'black-body' radiator at temperature T surrounds atoms in the flight tube, the frequency of the standard is shifted [11] according to:

$$\Delta\nu = \gamma\left(\frac{T}{300}\right)^4\left[1+\eta\left(\frac{T}{300}\right)^2\right] \qquad (4)$$

In order to evaluate the shift due to black-body radiation, the temperature of the vacuum vessel is monitored, and the published values of the coefficients γ and η [12] are used. NPL-CsF1 has four platinum resistors placed on the flight tube, two at the bottom and two at the top. The temperature measurement is traceable to the temperature scale at NPL. The peak-to-peak variation in the temperature of the vacuum vessel is less than 0.1 K. However, the lower part of the flight tube is warmer, by nearly 2 K, than the upper part due to the heat dissipated by the MOT coils. Taking this value as an estimate of the temperature uncertainty, the uncertainty of the shift due to black-body radiation is calculated to be 4×10^{-16}.

3.4 Microwave leakage

The frequency of NPL-CsF1 is shifted by the residual microwave field experienced by the atoms during the Ramsey time; the shift is linearly dependent on the microwave power. By changing the microwave field amplitude in the Ramsey cavity from $\pi/2$ to $11\pi/2$ (a power increase of a factor of 121), the extent of the shift is quantified (see fig.8). (The other shifts that depend on microwave power can be shown to be less than 10^{-16}. See Section 3.5.)

The difference in the shift for $\pi/2$ and $11\pi/2$ is found to be within ±30% of the average value over a 30 day period. This range is used to calculate the uncertainty due to microwave leakage. The value of the frequency shift, extrapolated to the $\pi/2$ level, is below 8×10^{-16} with an uncertainty of less than 3×10^{-16}.

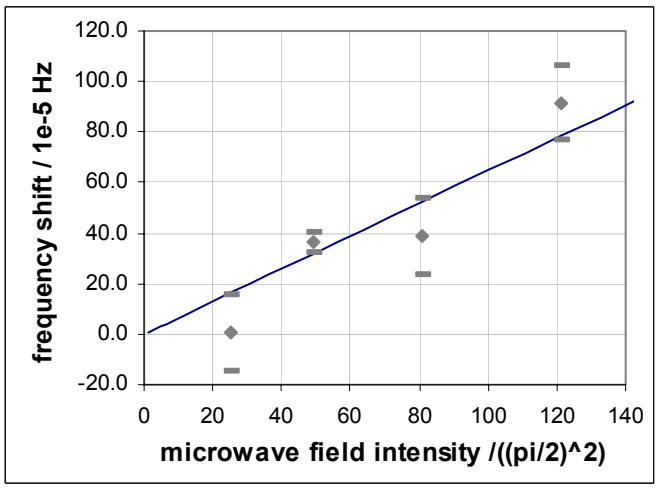

Fig. 8: Frequency difference NPL-CsF1–HM3 measured for microwave intensities corresponding to 5, 7, 9, and $11\pi/2$ pulses experienced by atoms in the Ramsey cavity.

3.5 Adjacent transitions, Rabi pulling, Ramsey pulling

The shift due to Rabi pulling is estimated following the analysis in [13]. After selecting the m_F=0 sublevel using the microwave selection pulse, the frequency applied to the Ramsey cavity is scanned over the transition frequencies of the other magnetic sub-levels. The populations of the $m_F\neq0$ sublevels are found to be less than 0.2% of the population of the m_F=0 sublevel. The Rabi pulling is calculated to be less than 10^{-20} and is omitted from the uncertainty budget.

Ramsey pulling is estimated using the approach developed in [14]. The worst case is considered; the m_F=1 and −1 atoms accumulate in the Ramsey interferometer asymmetric phases of π and $-\pi$, respectively. For the 1230 Hz separation of the $(0\rightarrow0)$ and $(1\rightarrow1)$ transition in NPL-CsF1 and the corresponding reduction of the $(1\rightarrow1)$ excitation to 4×10^{-4}, a negligible frequency shift of less than 10^{-16} is calculated.

3.6 Cavity pulling

The resonance frequency of the Ramsey cavity is offset from the atomic resonance by 800 kHz (±100 kHz). The offset is measured periodically. The cavity loaded Q is 12,500. The factional frequency shift is calculated using the theory presented in [15] to be 1×10^{-16}. The contribution to the cavity pulling due to the maser action of atoms in the cavity (radiation damping) is negligible for the number of atoms used [16].

3.7 Spectral impurities

The synthesis described in Section 2.3 contains spectral impurities (spurs) on the caesium resonance frequency; these are due to coupling of the phase locking loops to the ac supply (offset at harmonics of 50 Hz) and also to the 9.21 GHz DRO frequency and alternate sideband, from the output of the final mixer (offset at 17.368 and 34.736 MHz).

The spurs with offsets at 50 Hz and harmonics are more than 80 dB below the carrier and appear to be approximately the same on both sides of the carrier (double-sideband). The theory presented in [17] predicts a negligible shift in fractional frequency of less than 10^{-18} due to such a spur, in the worst case of it being a single-sideband spur.

The spur at 17.386 MHz offset has 20 dB higher power than the caesium resonance frequency. The theory [17] predicts a fractional frequency shift of several parts in 10^{15}. However, the relative amplitude of the field due to this spur is strongly reduced by the microwave cavity, resulting in a negligible shift in fractional frequency of a few parts in 10^{18}.

3.8 Distributed phase shift

The variation of the phase of the microwave field, in the horizontal plane, across the aperture in the Ramsey cavity results in a first order Doppler shift An estimate of the frequency shift is calculated by taking the worst-case values of the phase shift for a similar cavity [18] and accounting for the effect on the shift caused by the horizontal expansion of the atomic cloud. The vertical size of the atomic cloud is calculated from the effect produced by switching off the microwaves at a variable delay, relative to the launch. It is assumed that the horizontal and vertical size of the cloud is the same. The fractional frequency shift is estimated to be 3×10^{-16}.

3.9 AC Stark effect due to resonant light

During the Ramsey time, mechanical shutters, placed at the input of the optical fibres, block the laser beams used for cooling and detection. In order to estimate the AC Stark shift due to stray light coupled into the fibres, the fountain is operated alternately using two values of the laser detuning during the Ramsey time, 0.5 Γ and 10 Γ ($\Gamma = 2\pi\times5.3$ MHz). The measured frequency difference is consistent with zero within a statistical uncertainty of 2×10^{-15}. Thus, it is estimated that the AC Stark effect due to resonant light does not change the fractional frequency by more than $1\text{x}10^{-16}$.

3.10 Gravity

The fountain frequency is shifted by the gravity potential. The gravity potential is calculated from the height relative to the surface of constant gravity potential, the geoid (orthometric height) [19].

The orthometric height is obtained by two methods; from survey data relative to the Ordinance Datum Newlyn (ODM) (whose position is known relative to the geoid) and from extended GPS position data using a C/A code receiver. The GPS receiver provides height relative to the WGS84 ellipsoid. The model of the EGM96 geopotential, published by the NGA/NASA [20], was used to obtain the height difference between WGS84 and the geoid. The GPS-based measurement of the orthometic height agrees with the ODM-based height, which has an uncertainty of approximately 1 meter in the laboratory where NPL-CsF1 is housed. The uncertainty in the shift due to the gravity potential is estimated to be 1×10^{-16}

Effect	Bias ($\times10^{-15}$)	Uncertainty ($\times10^{-15}$)
2nd order Zeeman	142.7	<0.1
AC Stark (BBR)	-17.1	0.4
Collisions	-7.7	0.8
μ-w leakage	0.8	0.3
Cavity pulling	-	0.1
μ-w spectrum	-	<0.1
Cavity phase shift	-	0.3
Rabi, Ramsey pull.	-	0.1
AC Stark (lasers)	-	0.1
Gravity	1.6	0.1
Total (1σ)		1.0

Table 1: A summary of systematic effects considered in this evaluation together with their fractional frequency uncertainties.

4 Frequency measurements

The frequency of NPL-CsF1 is referenced to a hydrogen maser HM3, which in turn is linked to the maser HM1. HM1 is the master clock representing UTC(NPL) and is reported to BIPM by a two-way satellite time and frequency link (TWSTFT). The two masers are located 0.8 km apart and a 10

MHz link is maintained by an underground cable. The round-trip phase delay is continuously monitored, and demonstrates that the uncertainty in the fractional frequency, in relating the frequency of NPL-CsF1 to HM1, is negligible over a 30-day period. It is necessary to operate NPL-CsF1 in 30-day campaigns in order to reduce the satellite link uncertainty to less than 10^{-15} for one evaluation period. Two such campaigns have been completed (MJD 53054-53084 and 53089-53119).

During a campaign the fountain is run in the alternating mode between high and low atom number. The correction for the collisional frequency shift is calculated using a continuous set of 30 minute averages. Additional noise due to the correction procedure and the link between HM1 and HM3 results in a short-term stability of the NPL-CsF1–HM1 frequency difference of 6×10^{-13} in 1s, which means that a statistical uncertainty of 1×10^{-15} is reached after 4 days of averaging. Although the short-term stability is degraded by the continuous correction of the collisional shift, there is no reliance on long-term stability of the atom number or on any previously measured coefficient between the atom number and the collisional frequency shift.

Other than the collisional shift, the corrections are sufficiently stable over the campaign period for one value to be applied. However, the validity of that value is, in some cases, checked during a campaign. (All the corrections are checked at the start and end of a campaign. A detailed map of the magnetic field is made at these times.) The temperature of the vacuum vessel is recorded at one minute intervals. The microwave leakage level and the value of $\langle B \rangle$ for a 31 cm launch is checked every two days.

During the five-day period MJD 52995-53000, the NPL-CsF1 fountain was running simultaneously with the primary standard of the PTB (PTB CSF1). The two standards were compared using TWSTFT with the link dominating the uncertainty of the comparison. The fountains were found to agree within the uncertainty in the comparison.

5 Conclusions

A report on the construction and operation of the NPL-CsF1 fountain primary frequency standard has been presented. The NPL-CsF1 now realises the SI second with an uncertainty in the fractional frequency of 1×10^{-15}. The standard is contributing to the representation of TT, TAI and the reference to the SI second for optical frequency measurements at NPL.

It is planned to use NPL-CsF1 to improve the stability of UTC(NPL).

Acknowledgements

The authors thank Y. Ovchinnikov for assistance and helpful discussions and P. Whibberley for careful reading of the manuscript. This work was funded by the Time Programme of the UK National Measurement System.

References

[1] A. Clairon, G. Santarelli, S. Ghezali, P. Laurent, S. Lea, M. Bahoura, E. Simon, S. Weyers, K. Szymaniec, *Proc. 5th Symp. on Frequency Standards and Metrology* (World Scientific 1996) pp 49-59.

[2] S. Weyers, U. Huebner, R. Schroeder, Ch. Tamm, A. Bauch. *Metrologia,* **38**, pp. 343-352, (2001).

[3] S.R. Jefferts, J. Shirley, T.E. Parker, T.P. Heavner, D.M. Meekhof, C. Nelson, F. Levi, G. Constanzo, A. De Marchi, R drullinger, L. Hollberg, W.D. Lee, F.L. Walls. *Metrologia,* **39**, pp. 321-336, (2002).

[4] F. Levi, L. Lorini, D. Calonico, A. Godone. *IEEE Trans. Instr. Meas.,* **52**, pp. 267-271, (2003).

[5] K. Szymaniec, W. Chalupczak, D. Henderson. in *Proc.17th EFTF-FCS,* Tampa, Florida (2003).

[6] N.F. Ramsey. *Molecular Beams,* Oxford, (1956).

[7] S. Ghezali, P. Laurent, S.N. Lea, A. Clairon. *Europhys. Lett.,* **36**, pp. 25-30, (1996).

[8] P.J. Leo, P.S. Julienne, F.H. Mies, C.J. Williams. *Phys. Rev. Lett.,* **86**, pp. 3743-3746, (2001).

[9] F. Pereira, Dos Santos, H. Marion, S. Bize, Y Sortais, A. Clairon. *Phys. Rev. Lett.,* **89**, 233004, (2002).

[10] M. Arditi, T.R. Carver. *Phys. Rev.* **124**, pp. 800-809, (1961).

[11] W.D. Itano, L. Lewis, D. Wineland. *Phys. Rev. A,* **45**, pp. 1233-1235, (1982).

[12] E. Simon, P. Laurent, A. Clairon. *Phys. Rev. A,* **57**, pp. 436-439, (1998).

[13] J. Vanier, C. Audoin. *The Quantum Physics of Atomic Frequency Standards,* Adam Hilger, 1989, p. 835.

[14] L.S. Cutler, C.A. Flory, R.P. Giffard, A. De Marchi. *J. Appl. Phys.* Pp. 2780-2792, (1991).

[15] J. Vanier, C. Audoin. *The Quantum Physics of Atomic Frequency Standards,* Adam Hilger, 1989, p. 830.

[16] C. Fertig, K. Gibble. *Phys. Rev. Lett.,* **85**, pp. 1622-1625, (2000).

[17] J. Vanier, C. Audoin. *The Quantum Physics of Atomic Frequency Standards,* Adam Hilger, 1989, p. 818.

[18] A. Khursheed, G. Vecchi, A. De Marchi. *IEEE Trans. Ultrason. Ferroel. Freq. Contr,* **43**, pp. 201-210, (1996).

[19] N.K. Pavlis, M.A. Weiss. *Metrologia* **40**, pp. 66-73 (2003).

[20] http://earth-info.nga.mil/GandG/wgsegm/egm96.html